Journal of Crystal Growth 507 (2019) 321–326

Contents lists available at ScienceDirect

Journal of Crystal Growth

journal homepage: www.elsevier.com/locate/jcrysgro

Growth and fluorescence characteristics of Er:LuAG laser crystals

Jiliang Quan[b,c], Xin Yang[b], Siwei Long[b], Mingming Yang[b], Decai Ma[a], Jinqiang Huang[c], Yongwen Guo[c], Yunzhong Zhu[a,*], Biao Wang[a,b,*]

[a] Sino French Institute of Nuclear Engineering and Technology, Sun Yat-sen University, Zhuhai 519082, China
[b] School of Physics, Sun Yat-sen University, Guangzhou 510275, China
[c] Guangzhou Semiconductor Material Academy, Guangzhou 510610, China

ARTICLE INFO

Communicated by V. Fratello

Keywords:
A2. Single crystal growth
A2. Czochralski method
A1. Fluorescence characteristics
B1. Er:LuAG
B2. Laser material

ABSTRACT

Er-doped $Lu_3Al_5O_{12}$ (Er:LuAG) single crystals with various doping concentrations of 0.2, 0.5, 1.0, and 3.5 at% are grown by the Czochralski method. In the growth process, the cracking problem of this refractory crystal is overcome by a modified temperature field. Then, the lattice parameters and dopant segregation coefficient of as-grown boules are revealed. In addition to the structure and components, we mainly focus on the absorption and fluorescence spectra of Er:LuAG. Specifically, the absorption ranging from 250 to 1700 nm presents the characteristic energy-levels of the Er dopant. Using a 970 nm pump laser, strong fluorescence peaks are observed at 1532 nm, indicating Er:LuAG is an outstanding potential laser material in both the human eye-safe band and long air-path transmission. Notably, the best results were observed at an Er concentration of 1 at% with the highest luminescence intensity.

1. Introduction

Erbium-doped garnet single crystals, as excellent solid laser active media, have great potential for optical communication, medical surgery, remote sensor, and pumping sources of optical parametric oscillators (OPO) in infrared wavelength range [1–3]. Previous studies demonstrated that Er-doped garnets such as $Y_3Al_5O_{12}$ (YAG) and $Y_3Sc_2Ga_3O_{12}$ (YSGG) crystals present good thermal performance and high emission efficiency [4–6]. Furthermore, two types of laser output in high and low doping concentrations are discovered. Specifically, under high doping concentration (> 30 at%), the main radiation transfer between $^4I_{11/2}$ and $^4I_{13/2}$ levels can generate lasing in 2.7–3.0 μm wavelength, corresponding to the strong O–H absorption area [7]. On the other hand, when the Er concentration is low (0.5–2.0 at%) [8], the main transition level of $^4I_{13/2}$-$^4I_{15/2}$ can generate a laser wavelength around 1.5–1.67 μm, which meets the increasing demand of human eye-safe and long transmission distance [9]. Recently, Er-doped matrix materials (such as YAG, LuAG, YAP and YVO_4) for 1.5–1.67 μm solid lasers were well-studied [10–13]. Among them, Er:YAG is the most widely used laser active media with two emission wavelengths of 1617 and 1645 nm [14]. Unfortunately, the main emission wavelength of 1645 nm is located in the absorption region of methane, which severely shortens the laser transmission distance in air path (the absorption rate is $0.1\,km^{-1}$) [15]. Methane is a trace gas as well as the second largest greenhouse gas in the atmosphere. According to the World Meteorological Organization, the average concentration of methane in the global atmosphere reaches 1853 ppb [16]. On the other hand, another emission wavelength (1617 nm) of Er:YAG avoids the methane absorption, but its threshold population inversion is much higher than that of a 1645 nm laser [14]. Compared with YAG ($4.55\,g/cm^3$), LuAG possesses the advantage of higher density ($6.73\,g/cm^3$) which is more suitable for scintillation detectors [17]. Moreover, LuAG maintains good physical and chemical stability under long-term high intensity radiation and electron bombardment [18]. In addition, the lattice constant of LuAG (11.914 Å) is slightly smaller than that of YAG (12.008 Å) [19], which implies a stronger crystal field of LuAG than YAG. The stronger field can enhance the Stark effect, and its strength can be regarded as “stretching” energy level, namely, the higher the crystal field is, the stronger the stretching is [20]. This subtle enhancement can change the thermal populations of the upper and lower Er laser levels, and migrate the emission wavelength of Er:LuAG away from the conventional absorption peak of methane (1645 nm). Therefore, it is expected to be an ideal alternative crystal to Er:YAG with wide application prospects. However, LuAG single crystal requires a demanding growth environment. Its high melting point (2010 °C) deforms or even damages thermal insulation easily, resulting in an unstable temperature field. And the more difficult selection is the axial temperature gradient, since a large one cracks the crystal but a small one

---

* Corresponding authors at: Sino French Institute of Nuclear Engineering and Technology, Sun Yat-sen University, Zhuhai 519082, China (Y.Z. Zhu, B. Wang).
E-mail addresses: zhuyzh7@mail.sysu.edu.cn (Y. Zhu), wangbiao@mail.sysu.edu.cn (B. Wang).

https://doi.org/10.1016/j.jcrysgro.2018.11.037
Received 6 July 2018; Received in revised form 27 November 2018; Accepted 29 November 2018

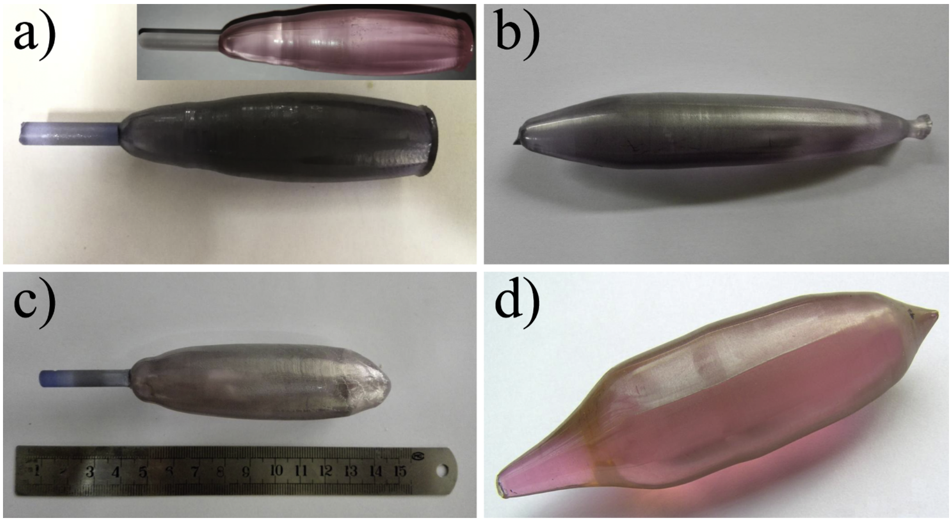

Fig. 1. Photographs of four as-grown Er:LuAG crystals with (a) 0.2 at%, (b) 0.5 at%, (c) 1.0 at%, and (d) 3.5 at% Er doping concentrations.

breaks the growth interface. Not only that, proper pulling and rotation rates are needed as well. Therefore, the growth work of such full-featured laser active media is still challenging, which results in many fewer reports on doped LuAG single crystals than its polycrystalline powder. On the basis of the outstanding performance of LuAG crystal, the doped LuAG series crystals have attracted wide attention in recent years [21–24]. However, up until now, there are few reports on the growth of full-size Er:LuAG single crystal boules by the Czochralski (Cz) method, only the related growth work of the micro pulling method and hydrothermal growth are reported [25,26].

It is known that rare earth doping determines the luminescence of a LuAG crystal, and the Er^{3+} concentration is crucial for the optical quality. But the optimal doping concentration has barely been investigated. Therefore, in this paper, we decide to grow Er:LuAG crystals with different doping concentrations. Then, based on numerical simulation, the modification work of the Cz temperature field is presented to solve the cracking problem. Most importantly, the optical absorption and emission properties of as-grown crystals in different doping concentrations will be discussed in detail. Thus, the optimal Er concentration stands out, and presents potential in both the human eye-safe band and long air-path transmission.

2. Experimental procedures

Er:LuAG crystals were grown by the Cz method with a radio-frequency heating system. The starting materials were Er_2O_3, Lu_2O_3, and Al_2O_3 with a purity of 99.999%. The three kinds of raw powders were dried at 300 °C for 10 h, and then weighed according to the formula $(Lu_{1-x}Er_x)_3Al_5O_{12}$ with $x = 0.002, 0.005, 0.01, 0.035$ (samples a-d). Then, the raw materials were mixed thoroughly, pressed into disks and calcined at 1300 °C for 48 h. After that, the crystals were grown in a DJL-50 furnace (XUT, China) in 2010 °C with an Ar atmosphere. ⟨1 1 1⟩-oriented LuAG bars were used as crystal seeds. The pulling and rotation rates were carefully selected to be 1–2 mm/h and 15–25 rpm, respectively. After growth, the as-grown boules were gradually cooled down to room temperature. As shown in Fig. 1a–d, four crack-free and scattering-free Er:LuAG single crystals with dimensions of $\phi 20 - 25 \times 80$ mm are obtained and present dark blue[1] color centers. We found that the color centers appear to decrease with the increasing doping concentrations. This phenomenon could be explained by the effects of the Er^{3+} dopant and the impurities produced by thermal insulation materials. Specifically, due to the lack of oxygen (in a pure inert atmosphere), it is easy to generate oxygen vacancies in the crystal growth duration. These vacancies will trap electrons to form an absorption band of a certain wavelength and result in obvious color center. However, the intrinsic absorption wavelength of Er will produce a different color (pink) when Er ions are doped into LuAG. As the doping concentration increases, the Er absorption intensity increases as well. Namely, the color center could be covered when the intrinsic color of the dopant becomes deep enough. On the other hand, impurities from the insulation materials will be attached to the surface of the boule. In our experiments, it takes several times to obtain a complete high-concentration Er:LuAG crystal. Since the impurities decrease gradually during the repetitive growth work, we found that the surface of the heavy-doped crystal is covered with much less impurities than that of the light-doped one. Then, as shown in the inset of Fig. 1a, since the oxygen annealing process can repair oxygen vacancies and oxidize impurities, the dark blue color center is eliminated by annealing in air for 48 h.

The post-annealing crystal boules were cut perpendicular to the growth direction in 1 mm thickness and polished on both sides. The lattice constants of Er:LuAG were identified using a X-ray diffractometer (XRD, Philips PW 3710) using Cu target Ka radiation. Furthermore, the Er concentration is measured by Inductively Coupled Plasma-Atomic Emission Spectrometric (ICP-AES, Ps-6, BAIRD) and used to determine the segregation coefficient. The absorption and fluorescence spectra were measured to characterize the optical properties of Er:LuAG. Specifically, the absorption spectra in the range of 250–1700 nm of the four Er:LuAG samples were recorded using a Perkin–Elmer Lambda-950 UV–VIS-NIR spectro-photometer with a spectral interval of 1 nm. The fluorescence spectra were measured from 1450 to 1660 nm by an Edinburgh fluorescence spectrometer (FLSP 920, spectral interval 0.5 nm) with an exciting source of a 970 nm laser diode (LD), and the corresponding fluorescence life-times of Er^{3+} ($^4I_{13/2}$ levels) were recorded with a Tektronix TDS420 oscilloscope under pulse excitation of a 970 nm laser.

3. Results and discussion

3.1. Growth condition optimization

The melting point of Er:LuAG is 2010 °C in the Cz system. With such high-temperature and longtime growth condition, it is easy to generate defects which seriously weaken the optical properties of the crystal. As

---

[1] For interpretation of color in Fig. 1, the reader is referred to the web version of this article.

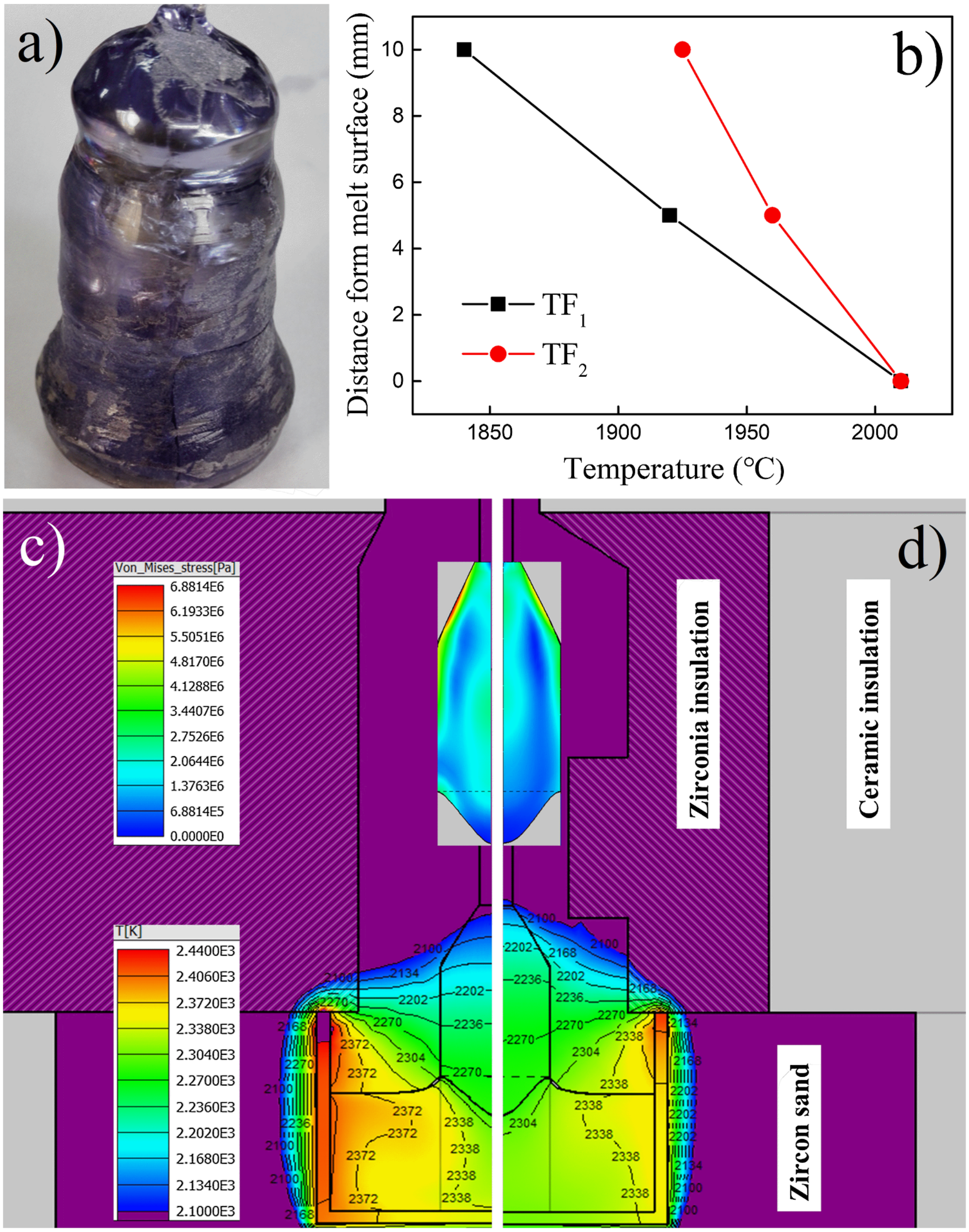

Fig. 2. (a) The full cracking Er:LuAG crystal. (b) The melt surface temperature fields of the original (TF_1) and modified (TF_2) growth conditions, the longitudinal axis represents the distance between temperature measuring points and liquid surface. (c, d) The computer simulation results of the original and modified crystal growth temperature fields. Zirconium oxide and ceramic materials are placed as double-layer insulation structure. The corresponding insets of (c) and (d) represent the respective inner stress fields of each boules during crystal growth.

shown in Fig. 2a, during our initial crystal growth work, cracking is a lingering problem in the shoulder and tail parts of the Er:LuAG crystal boule. The major reason for cracking is improper thermal insulation which results in a large temperature gradient and thermal stress in the crystal boule.

To prevent crystal cracking, we have taken the following measures.

(i) redesign the temperature field above the crucible: To maintain the optimum conditions of Er:LuAG growth, a large temperature gradient is required at the solid-liquid interface and a smaller temperature gradient above the melt is needed to prevent the crystal from cracking. Therefore, we designed a double-layer insulation structure above the crucible, which is more stable and possesses a lower temperature gradient than the single-layer insulation. At the same time, the sighthole maintains the large temperature gradient of the solid-liquid interface. Fig. 2b shows the measured temperature field above the melt surface of the cracking crystal (TF_1) and the modified one (TF_2), the axial temperature gradient above the melt was reduced from 18 to 10 °C/mm.

(ii) strictly controlled cone angle. The rapid cooling rate and crystal growth rate during shoulder process lead to high thermal stress, which is one of the important reasons for shoulder cracking of Er:LuAG crystal. We have tested and controlled the cone angle repeatedly, and confirm that the initial cone angle ranging in 30-60° can prevent the shoulder cracking effectively.

Similar adjustment work has been reported in our previous paper [27]. Moreover, the corresponding numerical simulation results of the poor and the modified temperature fields are shown in Fig. 2c and d, respectively (parameters are shown in Table 1). Comparing these two

Table 1
Parameters for the growth of Er:LuAG crystals.

Description (units, mm)	Original value	Modified value
Crucible inner radius	30	30
Crucible wall thickness	3	3
Crucible inner height	40	40
Thickness of crucible insulation at the bottom	60	60
Thickness of crucible insulation at the wall	58	58
Height of upper insulation	110	110
Inner radius of upper insulation	26	24
Inner radius of heat resistance	no	13
Thickness of upper insulation	65	65
Thickness of zirconia part in upper insulation	65	25
Thickness of ceramic part in upper insulation	0	40
Radius of heat dissipation hole	20	8
Coil inner radius	100	100
Coil thickness	8	8
Coil height	120	120

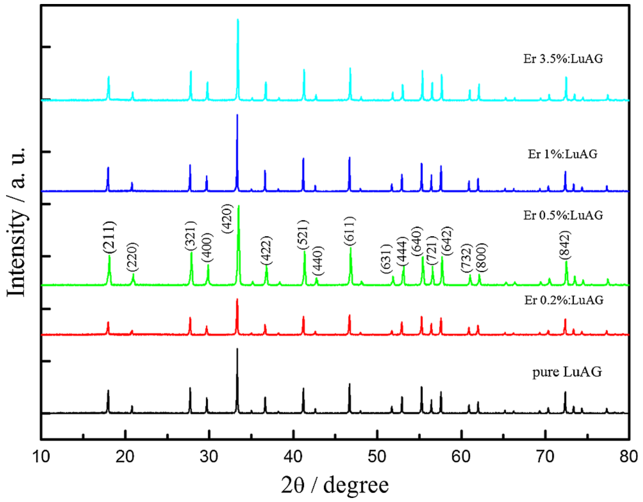

Fig. 3. The XRD patterns of pure LuAG and Er:LuAG single crystals in 0.2, 0.5, 1.0, and 3.5 at% doping concentrations.

Table 2
The lattice constants and effective doping concentrations (in crystal head and tail) of as-grown Er:LuAG crystal boules in different initial doping concentrations.

Samples	Lattice constant (Å)	Raw material (at%)	Head (at%)	Tail (at%)
a	11.9139 ± 0.0031	0.2	0.208 ± 0.011	0.199 ± 0.010
b	11.9141 ± 0.0035	0.5	0.495 ± 0.010	0.489 ± 0.009
c	11.9146 ± 0.0032	1	0.995 ± 0.009	1.011 ± 0.009
d	11.9158 ± 0.0036	3.5	3.511 ± 0.011	3.497 ± 0.010

figures, the effects of the modifications could be presented vividly. Specifically, as discussed above, the temperature gradient in Fig. 2c is large, which results in a more convex growth interface. Then, we adjusted the insulation system to reduce the temperature gradient and modify the growth interface. As shown in Fig. 2d, the upper heat dissipation hole is minimized, and a heat resistance part is added. Besides the temperature field, the insets (boule shape) of Fig. 2c and d represent the corresponding inner stress fields, respectively. These two cases clearly indicate the high and uneven stress field before the adjustment of the insulation system, and the moderate and uniform case after the adjustment. Through the above modifications, all the following crack-free LuAG crystal boules are obtained.

3.2. Structure and component characterization

The XRD patterns of the Cz-grown Er:LuAG crystals are shown in Fig. 3, including an undoped sample for comparison. The LuAG structure can be assigned from the sharp reflections. Furthermore, in the XRD spectra, all observed diffraction patterns correspond to the pure LuAG diffraction peaks, indicating a pure phase and good crystalline quality of the as-grown crystals. It is known that LuAG crystallizes in the garnet structure with a cubic space group of Ia-3d symmetry [17]. Specifically, in an Er:LuAG crystal, Er^{3+} ions could replace Lu^{3+} and enter the dodecahedron. Moreover, the lattice constants of the doped crystals are calculated from the XRD spectra as well, and the results are shown in Table 2. Since the ionic radii of Er^{3+} (1.004 Å) and Lu^{3+} (0.977 Å) are similar [25], the lattice constants of the Er:LuAG crystals are similar to that of pure LuAG (a_0 = 11.914 Å) [19]. In addition to the lattice constants, Table 2 also presents the Er doping concentrations of the head and tail parts of the as-grown boules measured by ICP-AES. One can point out that the original melt concentration of Er^{3+} ions is close to the head and the tail parts of the crystal boule. Thus, we can conclude that, in LuAG crystals, the segregation coefficient of Er^{3+} is close to 1.

3.3. Absorption spectra

Fig. 4 shows the energy levels of Er^{3+} and the absorption spectra of various Er:LuAG crystals in the wavelength range of 250–1700 nm. Although some absorption peaks overlap with adjacent energy levels and the background absorption is strong in 250–400 nm, among these crystals, the peaks position are similar and the typical absorption bands of Er^{3+} ion are obvious. Moreover, the intensities of the absorption peaks increase with the doping concentration, which is in accordance with previous reports [25].

Then, combining with the energy level diagram of Er^{3+} in Fig. 4a [25,28], we can analyze the overall absorption spectra thoroughly. As shown in Fig. 4b, the $^4F_{9/2}$ and $^4I_{9/2}$ absorption bands appear in the range of 635–685 and 780–860 nm, respectively. The $^4I_{11/2}$ band ranges from 940 to 1030 nm, and the absorption at 967.5 nm is the strongest. These broad absorption peaks imply the energy level splitting between ground and excited states. Under the influence of the crystal field in an Er^{3+} doped single crystal, the energy levels can split into several Stark energy levels that influence the radiative transition [29,30]. To discuss this phenomenon further, the absorption spectra of $^4I_{13/2}$ ranging from 1450 to 1650 nm are shown in Fig. 4c. Specifically, the absorption band from 1450 to 1500 nm is the result of the transition from ground state $^4I_{15/2}$ to the high energy state of $^4I_{13/2}$; and the absorption band from 1500 to 1550 nm corresponds to the transition from $^4I_{15/2}$ to the low energy state of $^4I_{13/2}$. The absorption spectra of these two intervals are strong and the spectral peaks are sharp. However, the absorption intensity in 1550–1650 nm is much smaller, corresponding to the transition from the high energy level of $^4I_{15/2}$ to the $^4I_{13/2}$ state. In general, because of this splitting phenomenon, all characteristic peaks of Er doped LuAG single crystals are more complex.

To investigate the emission spectra further, we prefer the absorption band of 967.5 nm, which matches the commercial InGaAs semiconductor laser. Moreover, the increased absorption coefficient and broad absorption band of the Er:LuAG crystal are suitable for the well-developed 970 nm LD pump source.

3.4. Emission spectra

It is known that doping concentration is an important factor for the output characteristics of laser materials. Generally speaking, the increase of the doping concentration is beneficial to the pump light absorption, laser threshold and output efficiency. But excessive dopant will increase the cross relaxation between ions, which induces the "bottleneck effect" and results in a huge decrease of output efficiency.

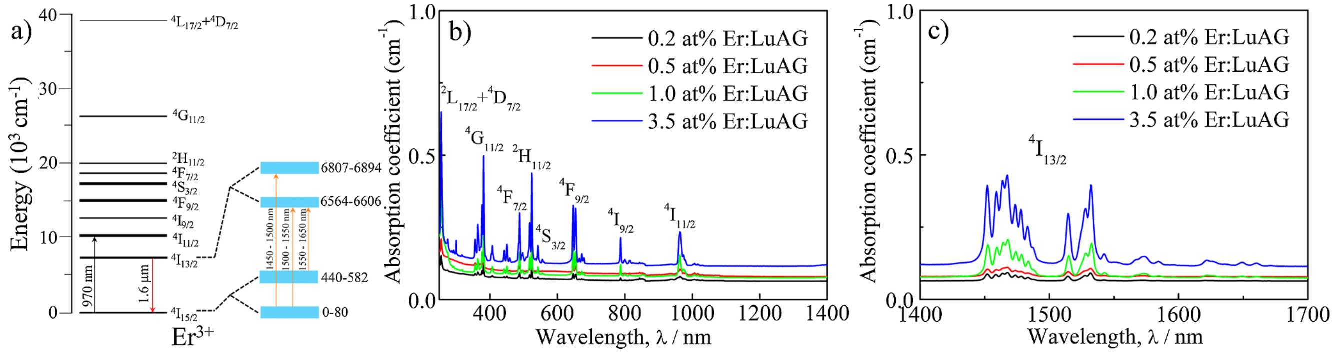

Fig. 4. (a) The energy level diagram of Er^{3+} ions in LuAG host crystal. (b) The absorption spectra of four Er:LuAG samples with different doping concentrations in 250–1400 nm and (c) 1400–1700 nm.

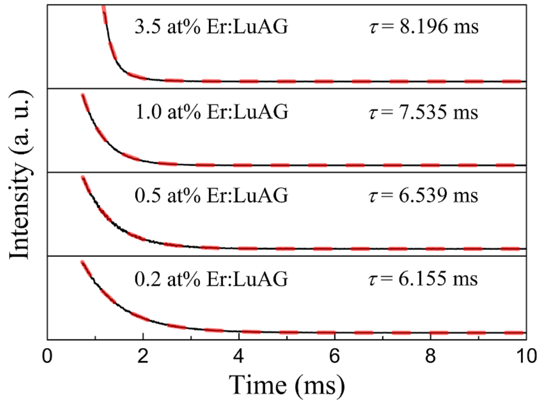

Fig. 5. Fluorescence decay curves of the $^4I_{13/2}$ levels of Er:LuAG crystals in different doping concentrations. The black solid curves are the measured data, and the red dotted ones are the fitted results. (For interpretation of the references to colour in this figure legend, the reader is referred to the web version of this article.)

Not only that, the self-reabsorption resulting from the overlap of $^4I_{13/2}$-$^4I_{15/2}$ emission and $^4I_{15/2}$-$^4I_{13/2}$ absorption would additionally decrease the emission around 1.5 μm [31]. Therefore, the optimal doping concentration should be carefully selected. For this purpose, we decided to study the fluorescence spectra of Er:LuAG crystals in different doping concentrations.

Fig. 5 shows the fluorescence decay curves of the $^4I_{13/2}$ levels of Er:LuAG crystals with different doping concentrations, and the fluorescence lifetime of the $^4I_{13/2}$ level is obtained by data fitting. The lifetime of the 0.5 at% Er:LuAG crystal is 6.539 ms, which is coincident with the calculated result of 6.7 ms [32]. Meanwhile, the fluorescence lifetimes of Er:LuAG crystals are enhanced with the increase of doping concentrations, and the tendency is similar to a previous report [33]. The fluorescence spectra of Er:LuAG crystals ranging from 1450 to 1660 nm under the 970 nm pump LD are shown in Fig. 6a and b. Four emission bands, exhibiting complex multiple peak structures, appear in the 1450–1650 nm region. Based on the Stark levels of Er^{3+}, we can determine that the observed four emission bands around 1450–1500, 1500–1550, 1550–1600 and 1600–1650 nm are assigned to the Er^{3+} transition of $^4I_{13/2}$ to $^4I_{15/2}$, and the strongest emission peak is located at 1532 nm. Despite originating from the same transition, these emission peaks (related to different Stark sub-levels transitions) are sharp and clearly separated from each other. This splitting phenomenon is considered to be useful in multi-wavelength IR emission devices. To compare two types of garnets further, Fig. 6c presents the fluorescence spectra of Er:YAG crystals ranging from 1600 to 1660 nm. One can find prominent emission peaks at 1617 and 1645 nm. However, compared with Er:YAG, the emission wavelength of Er:LuAG is shifted, and the main emission band is not close to the absorption peak of methane (1645 nm). It naturally solves the problem of methane absorption, which severely shortens the laser propagation distance in the atmosphere. The above results are encouraging and indicate that Er:LuAG is a promising potential candidate for NIR (near infrared) laser operation, which deserves further investigation.

The following discussion focuses on the influence of doping concentration on the fluorescence properties. According to Fig. 6a and b, the fluorescence intensity increases with the Er^{3+} doping concentration when it changes from 0.2 to 1 at%. However, when the concentration further increases to 3.5 at%, the fluorescence intensity becomes weak and the main emission peak migrates. When the doping concentration exceeds 1 at%, concentration-quenching and self-reabsorption dominate, indicating a significant interaction between Er^{3+}-Er^{3+} ions. Considering the above results, the best Er^{3+} doping concentration occurred at 1 at% where the crystal has the highest fluorescence intensity.

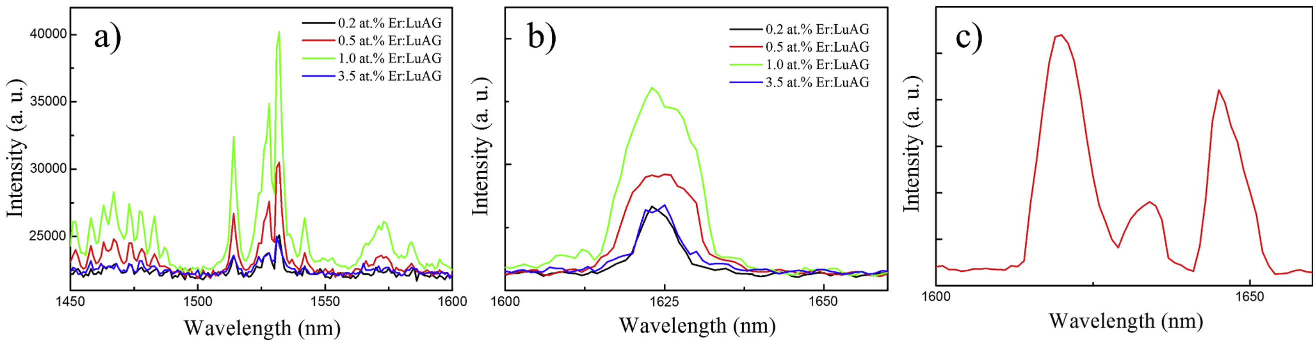

Fig. 6. (a, b) The fluorescence spectra in 1450–1600 and 1600–1660 nm of Er:LuAG crystals with four different doping concentrations. (c) The fluorescence spectrum of Er:YAG crystal in 1600–1660 nm.

4. Conclusions

Er:LuAG crystals with different doping concentrations were successfully grown by the Cz method. Cracking defects are analyzed and attributed to the large temperature gradient that leads to high heat stress and deformation, which can be eliminated by adjusting the temperature field and reducing the cone angle. Moreover, the optimization of the temperature field has been confirmed and presented by computer simulation as well. The powder XRD patterns indicate the pure phase and good crystalline quality of the as-grown crystals, and the corresponding lattice parameters are coincident with the pure LuAG crystal. Moreover, the ICP-AES results from the crystal head and tail prove the segregation coefficient of the Er^{3+} ion is approximately equal to 1. In addition to the structure and component studies, the absorption spectrum presents a strong absorption peak around 970 nm, which is suitable for 970 nm LD pumping. The most important point is that, the emission spectrum has a high fluorescence intensity for 1 at% Er:LuAG. However, when the doping concentration reaches 3.5 at%, concentration quenching occurs. Compared with the commonly used Er:YAG, Er:LuAG is an excellent alternative material, not only for its excellent physico-chemical properties, but also the proper luminous wavelength of both human eye safety and long-range atmospheric transmission.

Acknowledgements

This work was supported by the National Natural Science Foundation of China, China (NSFC) (Nos. 51802358, 11832019, 11372361), the National Natural Science Foundation of Guangdong Province, China (Nos. 2018A030313321, 2017A030310426), the Guangdong Science & Technology Project, China (2015B090927005) and the Fundamental Research Funds for the Central Universities, China (17lgpy37).

The authors would like to thank the Guangzhou Semiconductor Material Academy of Photoelectric Materials Research and Development Center for technical assistance in crystal growth.

References

[1] A. Zajac, M. Skorczakowski, J. Swiderski, P. Nyga, Electrooptically Q-switched mid-infrared Er:YAG laser for medical applications, Opt. Express 12 (2004) 5125–5130.
[2] H. Jelinkova, T. Dostálová, K. Hamal, O. Krejsa, J. Kubelka, S. Procházka, Er:YAG laser in dentistry, Laser Phys. 8 (1998) 176–181.
[3] D.M. Rines, G.A. Rines, P.F. Moulton, CdSe OPO pumped by a 2.79 µm Cr, Er:YSGG Laser, OSA Procee. Advanced Solid-State Laser 24 (1995) 184–186.
[4] B.J. Dinerman, P.F. Moulton, 3µm CW laser operations in erbium doped YSGG, GGG and YAG, Opt. Lett. 19 (1994) 1143–1145.
[5] D.W. Chen, C.L. Fincher, T.S. Rose, R.A. Fields, Diode-pumped 1-W continuous wave Er:YAG 3µm laser, Opt. Lett. 24 (1999) 385–387.
[6] Z.Y. You, Y. Wang, J.L. Xu, Z.J. Zhu, J.F. Li, H.Y. Wang, et al., Single-longitudinal-mode Er:GGG microchip laser operating at 2.7 µm, Opt. Lett. 40 (2015) 3846–3849.
[7] J. Su, C. Yang, Q.F. Li, Q.L. Zhang, J.Q. Luo, Optical spectroscopy of Er:YSGG laser crystal, J. Lumin. 130 (2010) 1546–1550.
[8] D.L. Sun, J.Q. Luo, Q.L. Zhang, J.Z. Xiao, W.P. Liu, S.F. Wang, Growth and radiation resistant properties of 2.7–2.8 µm Yb, Er:GSGG laser crystal, J. Cryst. Growth 318 (2011) 669–673.
[9] G.J. Koch, M. Petros, B.W. Barnes, J.Y. Beyon, F. Amzajerdian, J.R. Yu, et al., Validar: a testbed for advanced 2-micron Doppler lidar, SPIE 5412 (2004) 87–98.
[10] M. Němec, H. Jelínková, J. Šulc, K. Nejezchleb, V. Škoda, Resonantly pumped Er:YAG and Er:YAP lasers, Proc. of SPIE 7193 (2015) 71932P1–71932P6.
[11] V. Fromzel, N. Ter-gabrielyan, M. Dubinskii, Acousto-optically Q-switched, resonantly pumped, Er:YVO_4 laser, Opt. Lett. 21 (2013) 15253–15258.
[12] N.W.H. Chang, N. Simakov, D.J. Hosken, J. Munch, D.J. Ottaway, P.J. Veitch, Resonantly diode-pumped continuous-wave and Q-switched Er:YAG laser at 1645 nm, Opt. Express 18 (2010) 13673–13678.
[13] X.F. Yang, Y. Wang, H.T. Huang, D.Y. Shen, D.Y. Tang, A passively Q-switched Er:LuYAG laser with a grapheme saturable absorber, Laser Phys. Lett. 10 (2013) 105810.
[14] Y. Deng, B.Q. Yao, Y.L. Ju, X.M. Duan, T.Y. Dai, A diode-pumped 1617nm single longitudinal mode Er:YAG laser with intra-cavity etalons, Chin. Phys. Lett. 31 (2014) 074202.
[15] K. Fox, High-resolution spectra of isotopic methanes near 1645nm, Appl. Optics 23 (1984) 3040–3042.
[16] World Meteorological Organization, 2017: WMO Greenhouse Gas Bulletin, < http://www.wmo.int/pages/prog/arep/gaw/ghg/GHGbulletin.html > .
[17] E. Auffray, D. Abler, S. Brunner, B. Frisch, K. Arno, P. Lecoq, G. Mavromanolakis, et al., LuAG material for dual readout calorimetry at future high energy physics accelerators, IEEE. Nucl. Sci. 43 (2009) 2245.
[18] H.L. Li, X.J. Liu, L.P. Huang, Synthesis of lutetium aluminum garnet powders by nitrate- citrate sol- gel combustion process, Ceram. Int. 33 (2007) 1141–1143.
[19] E.V. Charnaya, C. Tien, T.Y. Her, Effect of substitutional order on the relaxation of aluminum nuclei in $Y_{(3-X)}Lu_XAl_5O_{12}$ mixed garnets, Phys. Solid State 45 (2003) 1672–1675.
[20] B.M. Walsh, G.W. Grew, N.P. Barnes, Energy levels and intensity parameters of Ho^{3+} ions in $Y_3Al_5O_{12}$ and $Lu_3Al_5O_{12}$, J. Phys. Chem. Solids 67 (2006) 1567–1582.
[21] M. Nikl, E. Mihoková, J.A. Mareš, A. Vedda, M. Martini, K. Nejezchle, et al., Traps and timing characteristics of LuAG:Ce^{3+} scintillator, Phys. Stat. Sol. A 181 (2000) R10–R12.
[22] K. Kamada, K. Tsutsumi, Y. Usuki, Crystal growth and scintillation properties of 2-inch-diameter Pr:$Lu_3Al_5O_{12}$ (Pr:LuAG) single crystal, IEEE. Trans. Nucl. Sci. 55 (2008) 1488–1491.
[23] M. Sugiyama, Y. Fujimoto, T. Yanagida, D. Totsuka, V. Chani, Y. Yokota, et al., Nd-doped $Lu_3Al_5O_{12}$ single-crystal scintillator for X-ray imaging, Radiat. Meas. 55 (2013) 103–107.
[24] A. Pirri, G. Toci, M. Nikl, V. Babin, M. Vladimir, Experimental evidence of a non-linear loss mechanism in highly doped Yb:LuAG crystal, Opt. Express 22 (2014) 4038–4049.
[25] M. Sugiyama, Y. Fujimoto, T. Yanagida, D. Totsuka, S. Kurosawa, Y. Futamia, et al., Crystal growth and scintillation properties of Er-doped $Lu_3Al_5O_{12}$ single crystals, Nucl. Instrum. Methods Phys. Res. A 664 (2012) 127–131.
[26] C.A. Moore, C.D. McMillen, J.W. Kolis, Hydrothermal growth of single crystals of $Lu_3Al_5O_{12}$ (LuAG) and its doped analogues, Cryst. Growth Des. 13 (2013) 2298–2306.
[27] J.L. Quan, X. Yang, M.M. Yang, D.C. Ma, J.L. Huang, Y.Z. Zhu, et al., Study on growth techniques and macro defects of large-size Nd:YAG laser crystal, J. Cryst. Growth 483 (2018) 200–205.
[28] S.D. Setzler, K.J. Snell, T.M. Pollak, P.A. Budni, Y.E. Young, E.P. Chicklis, 5-W repetitively Q-switched Er:LuAG laser resonantly pumped by an erbium fiber laser, Opt. Lett. 28 (2003) 1787–1789.
[29] Y.L. Zhou, X. Wang, J.P. Zhang, J.B. Han, Crystal field splitting and effective g factor of infrared emission band in Er^{3+}:YVO_4 single crystal, J. Mol. Struct. 1065–1066 (2014) 186–190.
[30] N. Ter-Gabrielyan, V. Fromzel, W. Ryba-Romanowski, T. Lukasiewicz, M. Dubinskii, Spectroscopic and laser properties of resonantly (in-band) pumped Er:YVO4 and Er:GdVO4 crystals: a comparative study, Opt. Mater. Express 2 (2012) 1040–1049.
[31] N. Jaba, M. Ajroud, G. Panczer, M. Férid, H. Maaref, Optical characterizations of Er^{3+}-doped $KLa(PO_3)_4$ phosphate crystals, Opt. Mater. 32 (2010) 479–483.
[32] P.X. Zhang, Z.Q. Chen, Y. Hang, Z. Li, H. Yin, S.Q. Zhu, Enhanced emission of the 1.50–1.67 µm fluorescence in Er^{3+}, Ce^{3+}-codoped $Lu_3Al_5O_{12}$ crystal, J. Alloys Compd. 696 (2017) 795–798.
[33] X.P. Qin, H. Yang, G.H. Zhou, D.W. Luo, Y. Yang, et al., Fabrication and properties of highly transparent Er:YAG ceramics, Opt. Mater. 34 (2012) 973–976.